Title

Insights from high-fidelity modeling of industrial rotary bell atomization

Journal

Proceedings of the National Academy of Sciences of the United States of America, 120(4)

ISSN

0027-8424

Authors

Saye, Robert I

Sethian, James A

Petrouskie, Brandon

et al.

Publication Date

2023-01-24

DOI

10.1073/pnas.2216709120

Peer reviewed

PNAS RESEARCH ARTICLE | APPLIED MATHEMATICS OPEN ACCESS

Insights from high-fidelity modeling of industrial rotary bell atomization

Robert I. Saye[a,1], James A. Sethian[a,b,1], Brandon Petrouskie[c], Aaron Zatorsky[d], Xinyu Lu[c], and Reza Rock[e]

Contributed by James A. Sethian; received September 30, 2022; accepted December 6, 2022; reviewed by David Chopp and Leslie Greengard

The global automotive industry sprayed over 2.6 billion liters of paint in 2018, much of which through electrostatic rotary bell atomization, a highly complex process involving the fluid mechanics of rapidly rotating thin films tearing apart into micrometer-thin filaments and droplets. Coating operations account for 65% of the energy usage in a typical automotive assembly plant, representing 10,000s of gigawatt-hours each year in the United States alone. Optimization of these processes would allow for improved robustness, reduced material waste, increased throughput, and significantly reduced energy usage. Here, we introduce a high-fidelity mathematical and algorithmic framework to analyze rotary bell atomization dynamics at industrially relevant conditions. Our approach couples laboratory experiment with the development of robust non-Newtonian fluid models; devises high-order accurate numerical methods to compute the coupled bell, paint, and gas dynamics; and efficiently exploits high-performance supercomputing architectures. These advances have yielded insight into key dynamics, including i) parametric trends in film, sheeting, and filament characteristics as a function of fluid rheology, delivery rates, and bell speed; ii) the impact of nonuniform film thicknesses on atomization performance; and iii) an understanding of spray composition via primary and secondary atomization. These findings result in coating design principles that are poised to improve energy- and cost-efficiency in a wide array of industrial and manufacturing settings.

rotary bell atomization | multiscale multiphase fluid flow | interface dynamics | higher-order numerics | high-performance computing

Significance

Industrial spray painting operations represent one of the most energy- and cost-intensive processes in modern manufacturing. Optimization of these processes would allow for improved robustness, reduced material waste, and significantly reduced energy usage. One of the few ways to gain insight into the spray formation itself, i.e., paint atomization, is through computational simulation; however, the sheer complexity of the underlying multiscale multiphysics poses significant challenges. In this work, we describe a high-fidelity mathematical and algorithmic framework to explore and analyze the intricacies of industrial-scale rotary bell atomization. Coupling state-of-the-art high-order numerics, laboratory-informed rheology, and high-performance supercomputing, our results have led to several key insights, unreachable through experiment alone.

In this paper, we introduce an integrated multiscale mathematical formulation and accompanying numerical methodology to accurately model the dynamics of rotary bell atomization. In rotary bell atomizers, Fig. 1, paint flows into a rapidly spinning bell and spreads across the inside surface, forming thin sheets and filaments at the edge, which then break apart into droplets shaped by externally applied air currents. From a physical, mathematical, and numerical point of view, this is a highly complex process. Typical bell rotation speeds vary from 10,000 to 70,000 rpm, creating tremendous centrifugal forces on paint films only tens of micrometers thick. Film and droplet breakup events occur over a submicrosecond timescale, yet computational simulations must run over many milliseconds to gather meaningful ensembles of droplets 10 to 100 μm in diameter compared to the centimeter-scaled bell. In addition, the non-Newtonian paint rheology is strongly affected by the extreme shearing rates, requiring robust handling of viscosity coefficients varying over multiple orders of magnitude.

To meet these challenges, we have developed a mathematical and numerical framework to model rotary bell dynamics over a wide range of industrially relevant physical parameters. Our model relies on an accurate solution of the complete bell/paint/gas dynamics, using a combination of tailor-made level set methods to track the liquid–gas boundaries of paint films and droplets as well as adaptive high-order discontinuous Galerkin methods to solve the underlying coupled liquid–gas non–Newtonian Navier–Stokes equations in a rotating coordinate system.

This work has been driven by a systematic interplay of mathematical modeling, numerical simulation, and laboratory experiment. Insights obtained include parametric trends in sheeting, filament, and droplet characteristics as a function of paint rheology, fluid delivery rate, and bell speed and geometry; atomization characteristics of both Newtonian and non-Newtonian shear-thinning paints; and findings concerning the role of film perturbations and primary/secondary atomization in the overall spray composition.

Reviewers: D.C., Northwestern University; and L.G., New York University.

Competing interest statement: The authors have organizational affiliations to disclose, B.P., A.Z., X.L., and R.R. work for PPG Industries, Inc.

[1]To whom correspondence may be addressed. Email: rsaye@lbl.gov or sethian@math.berkeley.edu.

This article contains supporting information online at http://www.pnas.org/lookup/suppl/doi:10.1073/pnas.2216709120/-/DCSupplemental.

Published January 18, 2023.

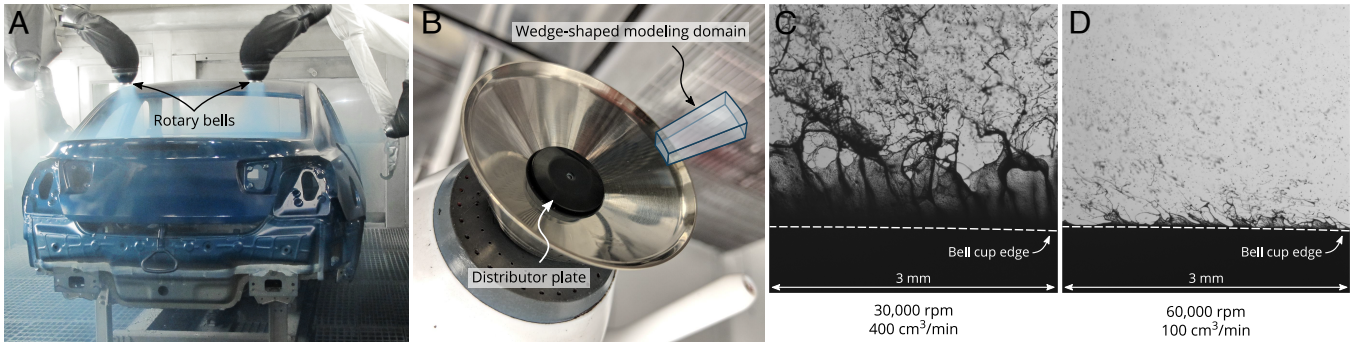

Fig. 1. Rotary bell atomization. (*A*) Electrostatic rotary bell atomizers are frequently used in industrial spray painting operations because of the high transfer efficiency and quality finish it provides. (*B*) Close-up of a typical bell. Paint is delivered behind the central distributor plate (black) and subsequently sheets across the rapidly rotating interior surface. (*C* and *D*) Pulsed laser illumination images of atomization at the bell edge. Atomization effectiveness is controlled in part by the bell rotation speed (indicated in rpm) and fluid delivery rate (cm^3 per minute) as well as the material properties of the paint.

1. Background

The application and cure of protective and decorative coatings is one of the most energy- and cost-intensive processes in modern industrial manufacturing. In the automotive manufacturing sector, for instance, paint shops account for 65% of the energy usage in a typical assembly plant (1, 2)—10,000s of gigawatt-hours each year in the United States alone. This energy usage is due largely to the tight temperature and humidity control required in the spray booth along with the application of multiple coating layers. While commonly used bells are capable of applying paint at 20% higher throughput than what is used in practice, as the fluid delivery rate is increased beyond its practical limit, the quality and consistency of the atomized paint are compromised, resulting in coating defects such as sag, air entrapment, and solvent popping during bake and cure. These defects require polishing and repainting of the affected part, reducing overall paint shop throughput and efficiency. A typical automotive paint shop runs with topcoat defect rates of 5% to 15%; any material or process improvements that reduce this have an immediate impact on the cost, energy efficiency, and environmental impact of painting a car (3).

Understanding the key fluid dynamics of paint film and filament formation, breakup, ejection, and droplet transport is crucial to optimizing the atomization process. However, computational fluid dynamics models previously used to study paint dynamics at the bell surface have been hindered by several factors, including the fast azimuthal bell speed, small film thicknesses and droplet sizes, intricate paint–gas coupling, and, in essence, insufficient computing power for low-order accurate models to converge at industrially relevant process conditions (4–9). This has ultimately led to a lack of resolution regarding many of the key driving mechanisms underlying rotary bell atomization. Combining high-order numerics, experimentally informed non-Newtonian models, and high-performance computing leads to models that uncover resolved dynamics at industrially relevant conditions.

2. Mathematical Formulation

The inherent circular symmetry in rotary bell atomization suggests a cylindrical coordinate system, $\mathbf{x} = r\hat{\mathbf{r}} + z\hat{\mathbf{z}} + \theta\hat{\boldsymbol{\theta}}$, in a reference frame attached to the rotating cup. We begin with the incompressible Navier–Stokes equations for the liquid (air+paint) dynamics, namely,

$$\rho_i\left(\mathbf{u}_t + \mathbf{u}\cdot\nabla\mathbf{u} + \boldsymbol{\omega}\times(\boldsymbol{\omega}\times\mathbf{x}) + 2\,\boldsymbol{\omega}\times\mathbf{u}\right) = -\nabla p + \nabla\cdot(2\mu_i\boldsymbol{\epsilon}),$$
$$\nabla\cdot\mathbf{u} = 0, \qquad [1]$$

where $\mathbf{u} = (u, v, w)$ describes the radial, azimuthal, and vertical components of the velocity field, p is the pressure, ρ_i and μ_i are the density and viscosity of fluid i, $\boldsymbol{\epsilon}$ is the rate-of-strain tensor (equal to $\frac{1}{2}(\nabla\mathbf{u} + \nabla\mathbf{u}^{\mathsf{T}})$ in a Cartesian coordinate system), and $\boldsymbol{\omega} = \omega\hat{\mathbf{z}}$ is the angular rotation of the cup. In the multiphase paint–gas system, one fluid phase is that of the paint, and the other is that of the surrounding air. The Navier–Stokes equations in each phase are coupled by the no-slip condition, $[\mathbf{u}] = 0$ on Γ, where Γ is the interface separating the two fluids, together with a jump condition on the stress tensor equaling the force of surface tension, $[\boldsymbol{\sigma}\cdot\boldsymbol{n}] = \gamma\kappa\boldsymbol{n}$, where $\boldsymbol{\sigma} = -p\mathbb{I} + 2\mu\boldsymbol{\epsilon}$ is the fluid stress, $\boldsymbol{n}$ is orthogonal to the interface, γ is the coefficient of surface tension, and κ is the mean curvature of the interface. Expanded equations for u, v, and w in the rotating coordinate system are detailed in (*SI Appendix*).

The computational domain is an angular wedge encompassing the edge of the cup, sketched in Fig. 1*B*; its shape is derived from cross-sectional cuts of industrial bells (*SI Appendix*, Figs. S1 and S2). Boundary conditions are prescribed to model the inflow of paint and shaping air nozzles on the outside surface of the bell as well as specially formulated outflow boundary conditions which permit droplets to flow away from the bell and exit the domain without impacting upstream dynamics; further details are given in *SI Appendix*.

A. Non-Newtonian Fluids. We need to develop a non-Newtonian fluid model that allows for typical paints and whose dynamics can be accurately and robustly approximated at extreme shearing forces. One standard approach is to adopt an Oldroyd-B model or similar; however, numerical approximations to these models are typically stable only for small Weissenberg numbers, far outside the regime appropriate for rapidly centrifuging paint films. Instead, we generated shear-strain profiles through experiment (*SI Appendix*, Fig. S10), developed numerical models of these profiles, and then compared numerical results with experiment. Through this process, we developed a general-purpose shear-thinning paint rheology framework, based on both power-law and modified Herschel–Bulkley models. In either case, the effective viscosity μ entering Eq. **1** varies as a function of the strain rate $\dot{\gamma}$, such that

$$\mu = k|\dot{\gamma}|^{n-1} + \tau_0|\dot{\gamma}|^{-1} + \mu_0,$$

where k, n, τ_0, and μ_0 are parameters describing the particular shear-thinning characteristics, and $|\dot{\gamma}|$ equals the Frobenius norm of the rate of strain tensor $\boldsymbol{\epsilon}$. Here, the power-law model ensues when τ_0 and μ_0 are both zero and is used in this work to isolate essential trends and characteristics of shear-thinning paints; on the other hand, the modified Herschel–Bulkley model corresponds to the case when all four parameters are nonzero, whose specific values have been fitted to commonly used waterborne latex-based automotive basecoats.

3. Numerical Framework and High-Performance Computing

To solve these equations, we developed a tailor-made numerical framework based on a hybrid finite difference level set method and high-order accurate multiphase multiphysics implicit-mesh discontinuous Galerkin methods. These methods combine structured octree grids with an implicit level set description of boundary and interface geometry along with discontinuous Galerkin (DG) methods and yield a sharp interface method capable of resolving interfacial dynamics in evolving geometries with high-order accuracy. Building on prior work (10, 11), here we coupled these methods to interface tracking algorithms to handle the intricate and complex topological changes inherent in the atomization process, along with a variety of additional techniques to tackle the challenging and computationally intensive physics at play. Some of the major aspects of this work include the following aspects. (Further details are given in *SI Appendix*.)

A. Hybrid Finite Difference Level Set and DG Methods. The air–paint interface is described using a level set formulation (12, 13), which seamlessly tracks droplet breakup and merging. We built a hybrid approach uniting the benefits of finite difference level set methods and high-order accurate DG methods for computing the fluid dynamics—the finite difference method uses extension velocities (14) computed with high-order accurate techniques (15) applied to the DG-computed fluid velocity and is implemented in a time-evolving narrow band (16) data structure that follows the movement of the interface. The hybrid approach allows sharp resolution of breakup and coalescence of thin films, filaments, and droplets of liquid.

B. Non-Newtonian Fluid Flow Solvers. The shear-thinning non-Newtonian liquids model specifies the local viscosity μ as a function of the local strain rate $\dot{\gamma}$ of the liquid. To solve the corresponding Navier–Stokes equations involving a nonlinear viscous stress term, we have developed a high-order accurate projection method-based algorithm. Briefly, a mixed explicit-implicit treatment is applied to the viscous operator wherein an implicit solve uses an effective viscosity $\mu = \mu(\dot{\gamma})$ evaluated at the beginning of the time step, where, in turn, the strain rate $\dot{\gamma}$ is estimated via the Frobenius norm of the rate of strain tensor $\frac{1}{2}(\nabla \mathbf{u} + \nabla \mathbf{u}^{\mathsf{T}})$, suitably reformulated in the rotating cylindrical

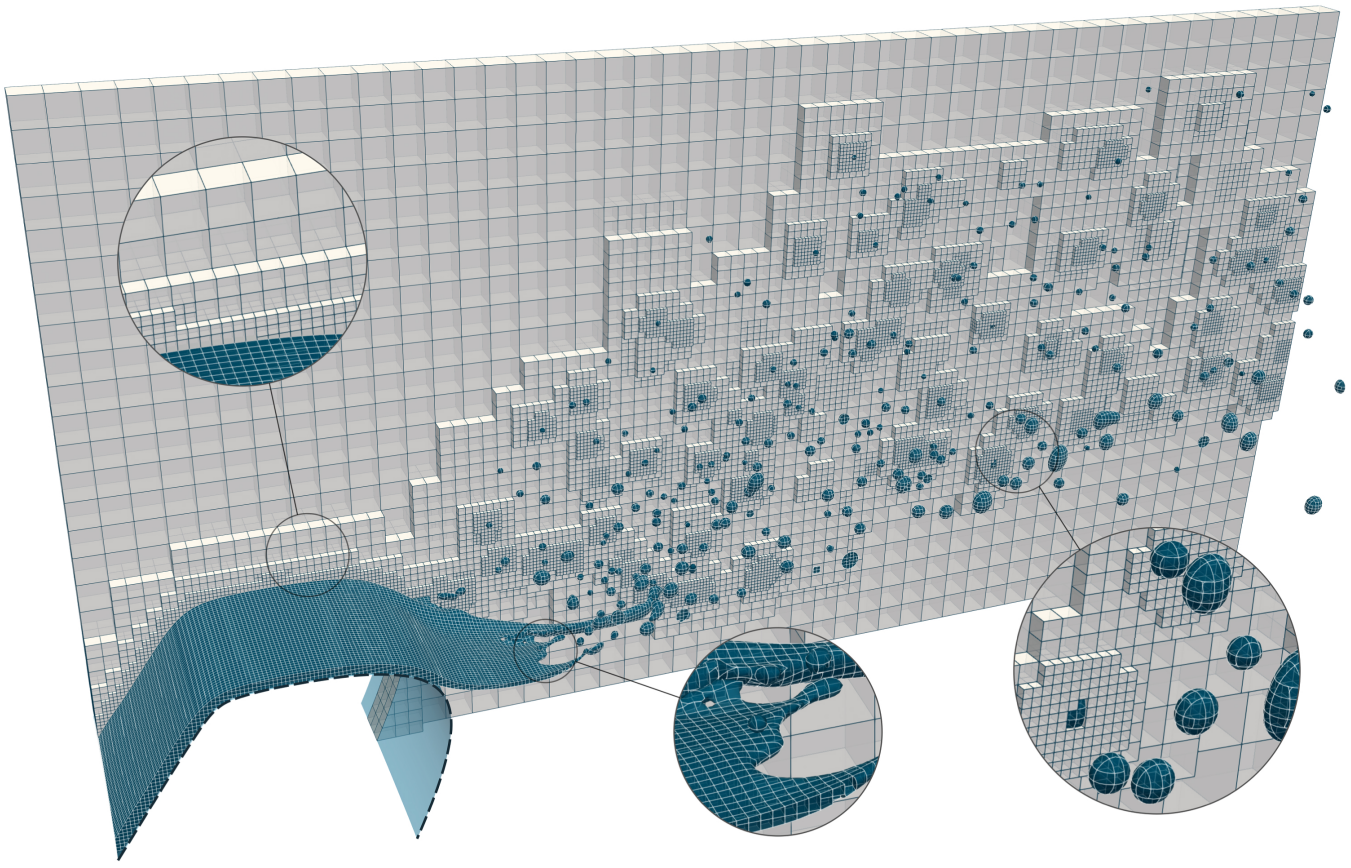

Fig. 2. Illustration of the adaptively refined mesh used in the numerical model. Elements in the liquid and gas phase are colored blue and gray, respectively (only a small subset of gas phase elements is shown so as to reveal the interior structure of the mesh); the dashed edge depicts the boundary of bell cup surface. Elements bordering the paint–gas interface have a smooth, curved, implicitly defined geometry, as determined by the multiphase cell cutting and merging procedure underpinning the high-order accurate implicit mesh DG method. Away from the paint–gas interface in the gas phase, the elements are relatively large; closer to the interface, the mesh is significantly refined so as to resolve small-scale features, such as droplet breakup dynamics and thin films and boundary layers.

coordinate system. This methodology also incorporates optimal-order accurate, variable-viscosity local discontinuous Galerkin schemes in cylindrical coordinates taking into account the interfacial stress jumps arising from surface tension forces. Numerical experiments indicated that the approach is high-order accurate, stable, and robust to a wide variety of shear-thinning models.

C. Adaptive Mesh Refinement Strategies. Because the liquid films, filaments, and droplets are so small, and the bulk gas phase is comparatively much larger, high-resolution modeling of atomization requires rather aggressive adaptive mesh refinement (AMR) strategies to focus computational accuracy where it is most needed. As shown in Fig. 2, the numerical model takes on a wide variety of elemental length scales, controlled by, among other aspects, the distance to the liquid–gas interface, the thickness of films, and the degree of interfacial curvature. This kind of refinement necessitates frequent updating of the AMR mesh; in typical simulations, remeshing is triggered as often as every five time steps.

D. Droplet Tracking. To examine the genesis and evolution of individual droplets, we have developed an algorithm tied to the DG method which analyzes and tracks the connected components of the liquid phase. The output of this algorithm is a directed graph of topology change events wherein i) each edge of the graph represents the lifetime of a single droplet and includes a temporal record of its center of mass, momentum, and angular momentum; while ii) each vertex represents a change in topology, e.g., the merger or breakup of specific droplets. With this graph, we can analyze how, when, and where droplets break up and merge (*SI Appendix*, Fig. S8), determine the ancestry of the final surviving droplets, and compute statistical distributions, e.g., of droplet sizes, velocities, and spinning (*SI Appendix*, Figs. S6 and S7).

E. High-Performance Computing. The advances presented here on high-fidelity atomization modeling stem in part from two complementary aspects: i) the use of tailor-made, high-order accurate numerical level set/DG methods and ii) their implementation on leadership-class high-performance computing facilities, including specialized domain decomposition and load balancing strategies as well as state-of-the-art solvers for the individual steps of the DG framework. As one example, we have made use of fast multigrid methods for elliptic equations in complex geometry (17–19); these methods make use of viscosity-upwinded numerical fluxes which can handle large viscosity/density variations several orders in magnitude, and their development was borne out of the present work.

4. Results

Our focus in this work is on modeling the primary atomization zone, including the lip of the bell and downstream a few millimeters, in an angular wedge portion of the cup, sketched in Fig. 1*B*. Our studies have predominantly used the Durr Ecobell 2 65-mm diameter smooth cup, representative of what is commonly used in the automotive industry to apply typical basecoat materials. The interior surface of this and many similar bells is a conic surface whose degree of incline impacts the sheeting and thin-film dynamics. This required development of a set of lubrication-style equations for centrifuging liquid films on rotating conic surfaces; these equations, derived in *SI Appendix*, are generalizations of similar equations found in the literature (20–22) and lead to equations predicting the film thickness h (together with its velocity profile u, v, w) such that

$$h = \left(\frac{3\mu Q}{2\pi c^3 \rho \omega^2 x^2}\right)^{\frac{1}{3}}, \qquad [2]$$

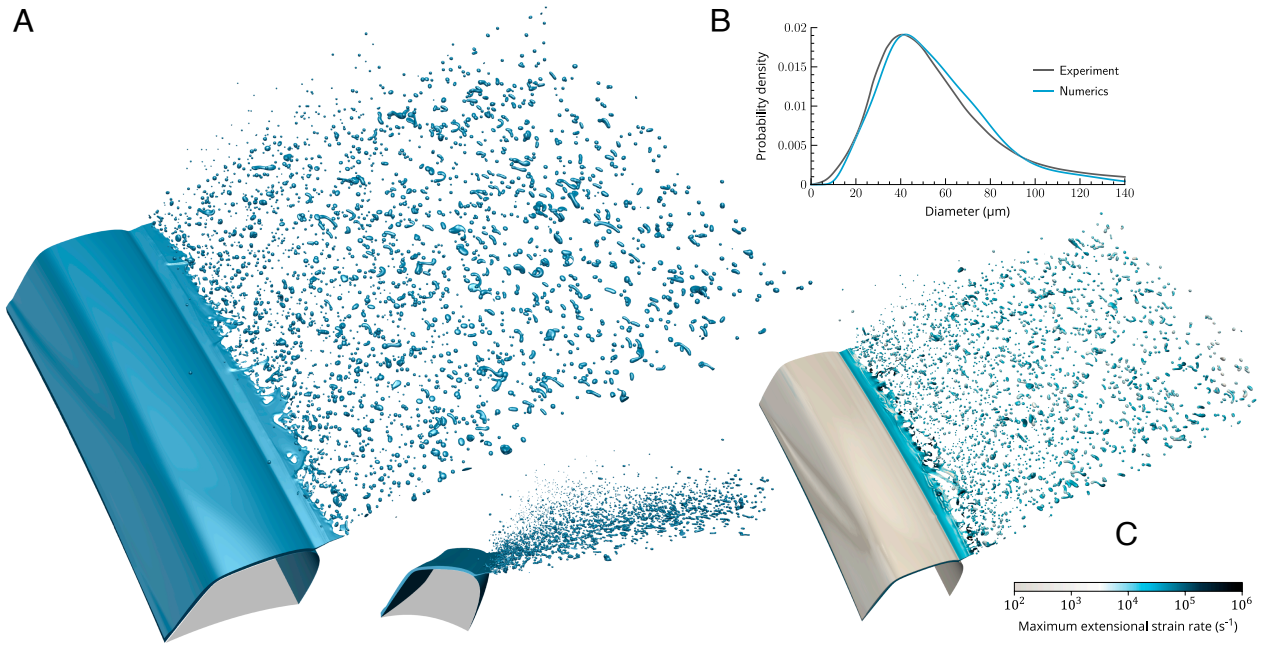

Fig. 3. Rotary bell atomization of Newtonian fluids. (*A*) Snapshot of numerical results. Liquid (blue) travels up the inside surface of the bell and over its beveled edge (shaded); after breaking apart, liquid droplets travel downstream to the right; the upward drift of the droplets as they fly away from the bell edge, as seen in the side-on view (*Inset*), is driven by shaping air currents. (*B*) Numerical and experimental volume-weighted droplet size distribution. (*C*) Maximal extensional strain rate on a logarithmic scale. (The gas phase is excluded from visualization.)

where $c = \cos\theta$ quantifies the conic incline and x is a tangential distance along the inside surface of the bell, for a film rotating at angular frequency ω, delivery inflow rate Q, Newtonian viscosity μ, and density ρ. A significant utility arising from these equations is that they allow us to specify inflow boundary conditions of the centrifuging liquid film as well as provide robust initial conditions for 2D axisymmetric simulations, whose solutions, in turn, provide an effective means of initializing fully 3D simulations; *SI Appendix* for details on this process.

In addition to non-Newtonian rheology, the study of atomizing Newtonian liquids played a key role in this work, in part to help with model verification, as well as to establish basic trends as a function of paint viscosity. We identified 1,3-butanediol as a suitable Newtonian liquid whose density ρ = 1.01 g cm^{-3} and surface tension γ = 47 g s^{-2} match with those of typical paints and whose viscosity μ = 100 cP matches with the high shear viscosity of a typical shear-thinning paint. With these parameters, Fig. 3*A* illustrates the results from one computational study for a bell rotating at 30,000 rpm. Liquid paint is seen to flow up the inside surface of the cup, travels over the beveled edge, where it then sheets and breaks apart into droplets, subsequently flying away downstream from the edge of the bell. Comparing the droplet size distribution predicted by the numerical model and an experimentally obtained droplet size distribution of a butanediol spray plume via laser diffraction analysis, encouraging agreement is seen (Fig. 3*B*). In addition to increased confidence in the model, these simulations provide insight into the typical strain rates exhibited by the atomizing liquid. For example, for the same process conditions as Fig. 3 *A* and *C* examines the maximum extensional strain rate of the butanediol liquid (as computed by the maximum eigenvalue of the rate of deformation tensor). These results indicate that the typical strain rates of the liquid, particularly near regions of breakup of the detaching sheet, can be one or two orders of magnitude higher than the strain rates witnessed by the smooth bulk film. This observation was important in determining a modified Herschel–Bulkley and power-law model for studying non-Newtonian shear-thinning paints.

The above study used a moderately large wedge (approximately 4.6°, corresponding to a bell edge arc length around 2.5 mm) and required moderately large computing resources. To more efficiently facilitate the parametric study of atomization behavior, we investigated the use of smaller wedges, i.e., decreasing the azimuthal extent of the computational domain. However, there

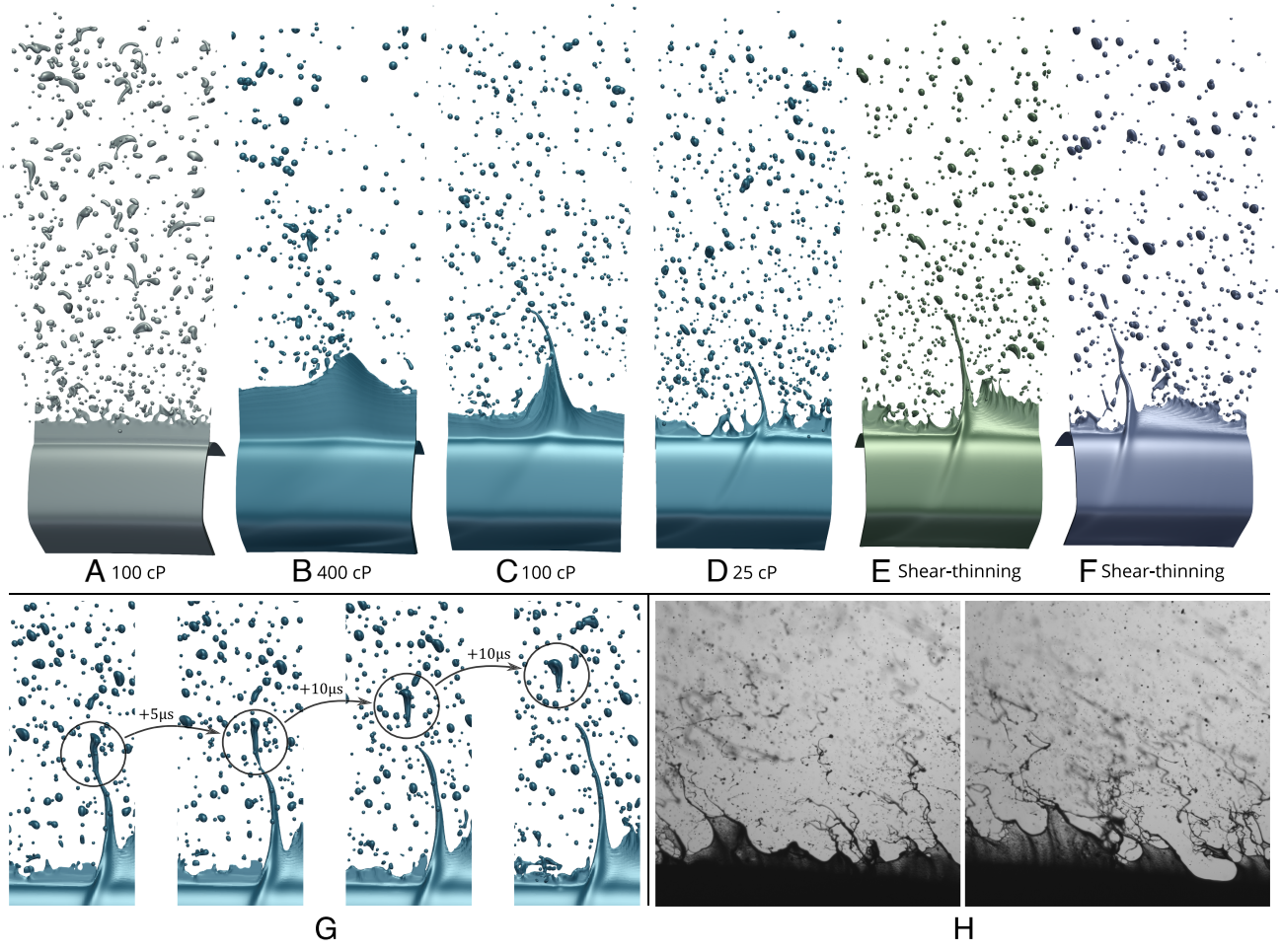

Fig. 4. Sheeting characteristics resulting from variations in inflow film thickness. (*A*) Reference example in which no variations in film thickness occur. (*B–F*) Example results for three Newtonian and two shear-thinning liquids. Here, a sinusoidal variation of equal amplitude is prescribed in the inflow film thickness on the interior of the bell; the degree to which this variation is dampened or amplified on the beveled edge depends on the viscosity. Note: All six examples, (*A–F*), apply the same process conditions, in particular, a fluid delivery rate of 300 ccm and bell speed 30 krpm. (*G*) Temporal sequence showing the detachment of a large droplet from the end of a filament; the time delta between frames is indicated. (*H*) High-speed imaging of atomizing butanediol; 300 ccm and bell speed 30 krpm, each frame is 3 mm by 3 mm.

is a tradeoff between the spatial and temporal domain size: as the angular extent is made smaller, longer simulation time horizons are required in order to atomize enough droplets for meaningful statistics. Furthermore, if the wedge size is excessively small, then the azimuthal periodic boundary conditions employed by the model can overconstrain the dynamics, leading to unphysical results. *SI Appendix* describes a computational study of wedge angle size whose results indicate that a wedge about half the size of Fig. 3 offers a good compromise. This wedge size was used in the subsequent results presented below.

Our computational studies of rotary bell atomization examined a wide arrange of aspects, including bell speeds and fluid delivery rates; rheological parameters such as density, surface tension, viscosity, and shear-thinning characteristics; the impact of film disturbances on sheeting and filaments; and the role of shaping air currents as well as bell geometry. Executed on leadership-class supercomputing facilities such as ALCF's Theta, NREL's Peregrine & Eagle, and NERSC's Edison & Cori supercomputers, the development of the numerical framework and subsequent parametric studies totaled to around 100 million core-hours of compute time. Among these studies, two particularly notable facets were identified, helping to shed light on the intricacies of rotary bell atomization. These facets are discussed in the next two sections. (*SI Appendix* which contains additional parametric studies and results.)

A. Effects of Inflow Film Thickness Perturbations. In practical settings, the film traveling over the edge of the bell is typically not uniform in thickness (7, 9, 23, 24). There are various causes for this, including, primarily, the impact of the distributor plate at the center of the bell (Fig. 1*B*); see also *SI Appendix*, Fig. S9, which shows experimental highspeed footage of nonuniformities on the bell interior surface. A consistent trend observed in all of our computational modeling results is that localized thickness variations create nonuniformities in the detaching film, which, in turn, promote the creation of uncontrolled filaments having poor atomization qualities. To study this effect, we altered the inflow boundary conditions Eq. **2** such that Q is a sinusoidal function of the azimuthal coordinate: This creates a sinusoidal film thickness in the prescribed incoming film. Fig. 4 shows one such study. In general, for shear-thinning liquids or Newtonian liquids with small viscosity, thickness variations on the inside surface of the bell tend to be amplified as they travel over the edge, creating pronounced localized ridges of paint which, in turn, create filaments. (Only if the liquid viscosity is sufficiently large are these disturbances smoothed out, Fig. 4*B*.) Characteristics like this are also witnessed in laboratory experiment: Fig. 4*H* shows images taken via in situ pulsed laser imaging of atomizing butanediol under the same fluid delivery rate and bell speed. Note the similarity with numerical results. A visual inspection of the simulation results shows that large blobs of liquid tend to travel down the filament (Fig. 4*G*) and then pinch off, creating outliers in droplet size distribution. From these observations, we surmise that nonuniformities in the sheeting behavior inside the surface of the ball play a distinct role in creating large, uncontrolled detaching films and filaments, which, in turn, contribute to unwanted outliers in droplet size distributions.

B. Primary and Secondary Droplet Composition. Besides being able to track the trajectory and local spinning of individual droplets (*SI Appendix* for a parametric study of these features), the liquid-phase connected-component analysis produces a wealth of data, permitting the study of merger and breakup events as well as determining the origin of the spray's final-surviving droplets. Here, we define "primary droplets" as those directly ejected by the bulk liquid component, while "secondary droplets" are those that arise from the merger or breakup of existing droplets. Our droplet composition analysis across several parametric studies revealed three notable aspects: i) primary droplets are typically smaller than secondary droplets, with secondary droplets making up the bulk of the tail-end of the volume-weighted droplet distribution (demonstrated, e.g., in Fig. 5); ii) among secondary droplets, by count, more of them are created via breakup mechanisms than by merger of existing droplets; and iii) the larger the effective viscosity of the liquid, the larger the fraction of secondary droplets in the resulting spray, for both Newtonian and shear-thinning liquids (also demonstrated in Fig. 5).

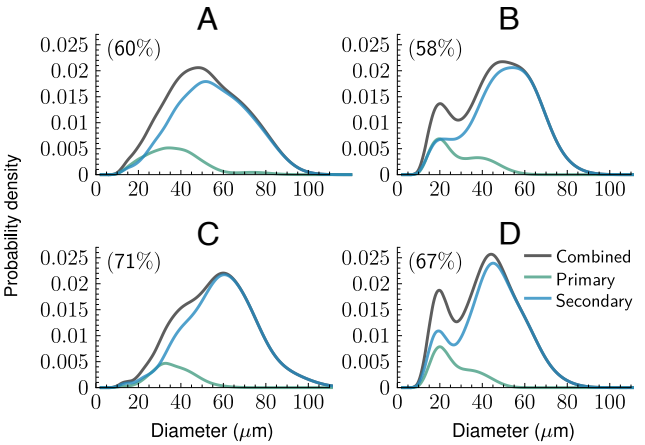

Fig. 5. Impact of the effective fluid viscosity on droplet composition. Volume-weighted droplet distribution of primary (green curve) and secondary (blue curve) droplets, whose combined total (black curve) is normalized to have unit integral. In each case, the percentage figures in parentheses indicate how many of the final-surviving droplets are of secondary type. (*A*) and (*C*): Butanediol and a Newtonian liquid of viscosity four times larger, respectively, at a fluid delivery rate of 300 ccm and bell rotation speed 30 krpm. (*B*) and (*D*) Two shear-thinning liquids, in which the second is more rapidly thinning but higher effective viscosity than the first, at a fluid delivery rate of 300 ccm and bell rotation speed 45 krpm.

5. Industrial Insights

Here, we summarize the implications of these results.

A. Primary vs. Secondary Atomization. Previous experimental studies indicate that primary atomization is the dominant mode of droplet breakup in the rotary bell atomization process; on the other hand, some previous computational studies indicate that secondary atomization may also be contributing to the overall droplet population (6, 7, 9). Through direct comparison of simulated droplet distributions to experimental results, this work has confirmed that a large percentage of atomized droplets stem from one or more secondary atomization events. This points to a strategy of adjusting the rheological properties of automotive paint to more easily undergo secondary atomization so as to improve atomization and performance under high throughput spray processes.

B. Stage-Dependent Shear. The numerical approach quantifies the strain rate range that the fluid experiences in each stage of the atomization process and reveals that the relevant strain rates during the spray process are a factor of 100 larger than those probed with the cone and plate rheometers typically used

to measure flow of coatings during development. Improved characterization techniques in this strain rate regime will allow for better paint rheology design for improved atomization, while maintaining critical performance properties such as smoothness and sag resistance.

C. Disturbances in Film Thickness. Lastly, fluid perturbations on the bell cup surface during spray were found to significantly impact atomization behavior. Large perturbations were found to result in broader droplet size distributions, known to result in worse appearance and defect performance in real spray applications. Based on these findings, future efforts will be directed at reducing these perturbations through equipment or paint design, which will result in more uniform droplet distributions and more robust and consistent coating performance.

6. Concluding Remarks

Automotive manufacturers are quickly moving to higher-throughput paint application processes to reduce energy consumption and cycle time in manufacturing. However, doing so often leads to poor paint atomization, resulting in appearance deficiencies and increased tendency for defect formation, leading to reduced quality and shorter lifetime. Innovative automotive coating technologies are necessary to overcome these deficiencies. Through high-fidelity numerical simulation, a number of key findings, unreachable through experimental approaches alone, have yielded insight into the key dynamics and characteristics of rotary bell atomization. These findings have resulted in better coating design principles, suggesting innovative solutions which improve process robustness, quality, and efficiency in these energy- and cost-intensive industrial coating operations.

The high-order numerical framework and modeling approaches developed here could be extended to include a host of additional phenomena important in industrial settings. As one example, we concentrated here on smooth bells; serrated or grooved bells are also commonplace and can result in different atomization characteristics regarding filament formation, air entrapment, and coating appearance. Also concerning bell geometry, the distributor plate is expected to play a key role in the formation of nonuniform film thicknesses (7, 9); in future work, we plan to directly couple injection, distributor plate, interior surface, and bell edge liquid dynamics so as to develop a more complete picture of film disturbances on atomization performance. Meanwhile, in electrostatic rotary bell atomization, electrical charges in the liquid and the short-to-long-range forces coupling them can alter atomization behavior, particularly in secondary breakup and their flight path toward the target; a further advance would be to incorporate the additional multiphysics arising in electrohydrodynamic atomization. Additional avenues include modeling particulates in the paint (e.g., metallic flakes) as well as air entrapment effects. Finally, there is a promising potential to steer and automate these kinds of high-fidelity simulations of atomization by coupling them to surrogate-based reduced order modeling; such an approach could pave the way to further innovative solutions in industrial coating operations and related areas in manufacturing.

Data, Materials, and Software Availability. All study data are included in the article and/or *SI Appendix*.

ACKNOWLEDGMENTS. This research was supported in part by the Applied Mathematics Program of the US Department of Energy (DOE) Office of Advanced Scientific Computing Research under contract number DE-AC02-05CH11231, by a DOE Office of Science Early Career Research Program award, and by the High Performance Computing for Manufacturing program sponsored by the US DOE Advanced Manufacturing Office of the Energy Efficiency and Renewable Energy Office under Contract DE-AC02-05CH11231, Cooperative Research and Development Agreement (CRADA) FP00005092, and CRADA FP00006835. Some computations used resources of the Argonne Leadership Computing Facility, which is a DOE Office of Science User Facility supported under Contract DE-AC02-06CH11357. Some computations were performed using computational resources sponsored by the Department of Energy's Office of Energy Efficiency and Renewable Energy and located at the National Renewable Energy Laboratory. Some computations used resources of the National Energy Research Scientific Computing Center, a US Department of Energy Office of Science User Facility at Lawrence Berkeley National Laboratory, operated under Contract No. DE-AC02-05CH11231. The government, PPG Industries, Inc., and Lawrence Berkeley National Laboratory make no express or implied warranty as to the conditions of the research or any intellectual property, generated information, or product made or developed under this CRADA, or the ownership, merchantability, or fitness for a particular purpose of the research or resulting product. Neither the government, PPG Industries, Inc., nor Lawrence Berkeley National Laboratory shall be liable for special, consequential, or incidental damages.

Author affiliations: [a]Mathematics Group, Lawrence Berkeley National Laboratory, Berkeley, CA 94720; [b]Department of Mathematics, University of California, Berkeley, CA 94720; [c]Materials Science and Engineering Group, PPG Industries Coatings Innovation Center, Allison Park, PA 15101; [d]Process Engineering Group, PPG Industries Springdale Research, Springdale, PA 15144; and [e]Protective Coatings Formulation Science, PPG Industries Coatings Innovation Center, Allison Park, PA 15101

Author contributions: R.I.S., J.A.S., B.P., A.Z., X.L., and R.R. designed research; performed research; analyzed data; and wrote the paper.

1. A. Kumar, Automotive coatings: Technologies and global markets (Tech. rep., BCC Research, 2019).
2. A. Giampieri, J. Ling-Chin, Z. Ma, A. Smallbone, A. Roskilly, A review of the current automotive manufacturing practice from an energy perspective. *Appl. Energy* **261**, 114074 (2020).
3. E. H. Tong, T. A. Loch, "Paint usage reduction in automotive paint booths" in *SAE 2000 World Congress* (SAE International, 2000).
4. K. Luo, C. Shao, M. Chai, J. Fan, Level set method for atomization and evaporation simulations. *Prog. Energy Combust. Sci.* **73**, 65–94 (2019).
5. J. Domnick, Z. Yang, Q. Ye, "Simulation of the film formation at a high-speed rotary bell atomizer used in automotive spray painting processes" in *22nd Annual Conference of ILASS-Europe on Liquid Atomization and Spray Systems, Como Lake, Italy. Paper ID ILASS08–A009* (2008).
6. L. A. Martinez, Master's thesis (University of Gothenburg, 2011).
7. A. J. Salazar, "Computational modeling of relevant automotive rotary spray painting process" in *Automotive Painting Technology*, K. Toda, A. Salazar, K. Saito, Eds. (Springer, Netherlands, 2012), pp. 47–95.
8. N. Guettler, P. Knee, Q. Ye, O. Tiedje, Initial droplet conditions in numerical spray painting by electrostatic rotary bell sprayers. *J. Coat. Technol. Res.* **17**, 1091–1104 (2020).
9. B. Shen, Q. Ye, N. Guettler, O. Tiedje, J. Domnick, Primary breakup of a non-Newtonian liquid using a high-speed rotary bell atomizer for spray-painting processes. *J. Coat. Technol. Res.* **16**, 1581–1596 (2019).
10. R. Saye, Interfacial gauge methods for incompressible fluid dynamics. *Sci. Adv.* **2** (2016).
11. R. Saye, Implicit mesh discontinuous Galerkin methods and interfacial gauge methods for high-order accurate interface dynamics, with applications to surface tension dynamics, rigid body fluid-structure interaction, and free surface flow: Part I. *J. Comput. Phys.* **344**, 647–682 (2017).
12. S. Osher, J. A. Sethian, Fronts propagating with curvature-dependent speed: Algorithms based on Hamilton-Jacobi formulations. *J. Comput. Phys.* **79**, 12–49 (1988).
13. J. A. Sethian, *Level Set Methods and Fast Marching Methods: Evolving Interfaces in Computational Geometry, Fluid Mechanics, Computer Vision, and Materials Sciences* (Cambridge University Press, London, 1999).
14. D. Adalsteinsson, J. A. Sethian, The fast construction of extension velocities in level set methods. *J. Comput. Phys.* **148**, 2–22 (1999).
15. R. I. Saye, High-order methods for computing distances to implicitly defined surfaces. *Commun. Appl. Math. Comput. Sci.* **9**, 107–141 (2014).
16. D. Adalsteinsson, J. A. Sethian, A fast level set method for propagating interfaces. *J. Comput. Phys.* **118**, 269–277 (1995).
17. D. Fortunato, C. H. Rycroft, R. Saye, Efficient operator-coarsening multigrid schemes for local discontinuous Galerkin methods. *SIAM J. Sci. Comput.* **41**, A3913–A3937 (2019).
18. R. I. Saye, Efficient multigrid solution of elliptic interface problems using viscosity-upwinded local discontinuous Galerkin methods. *Commun. Appl. Math. Comput. Sci.* **14**, 247–283 (2019).

19. R. I. Saye, Fast multigrid solution of high-order accurate multiphase Stokes problems. *Commun. Appl. Math. Comput. Sci.* **15**, 147–196 (2020).
20. J. O. Hinze, H. Milborn, Atomization of liquids by means of a rotating cup. *J. Appl. Mech.* **17**, 145–153 (1950).
21. T. G. Myers, M. Lombe, The importance of the Coriolis force on axisymmetric horizontal rotating thin film flows. *Chem. Eng. Process.: Process Intensif.* **45**, 90–98 (2006).
22. K. R. J. Ellwood, J. L. Tardiff, S. M. Alaie, A simplified analysis method for correlating rotary atomizer performance on droplet size and coating appearance. *J. Coat. Technol. Res.* **11**, 303–309 (2014).
23. S. Kazama, Steady-state paint flow under high centrifugal force: Atomization in spray painting. *JSAE Rev.* **24**, 489–494 (2003).
24. S. Ogasawara *et al.*, Liquid atomization using a rotary bell cup atomizer. *J. Fluid Sci. Technol.* **5**, 464–474 (2010).